

A maximum entropy approach to optimal mixing in a pulsed source–sink flow

Mark A. Stremler and Baratunde A. Cola^{a)}

Department of Mechanical Engineering, Vanderbilt University, Nashville, Tennessee 37235-1592

(Received 25 August 2005; accepted 17 November 2005; published online 6 January 2006)

Fluid mixing in a Hele–Shaw cell can be accomplished by periodically pulsing pairs of sources and sinks. The mixing efficiency of this system depends largely on the volume of fluid that is injected (and extracted) during each pulse. In this paper, the authors use a two-dimensional potential flow model to find the pulse volumes that optimize mixing in a rectangular domain containing two source–sink pairs, a system of current interest in DNA microarray analysis. Optimal mixing protocols are identified by determining maximum entropy using an analysis of chaotic advection.

© 2006 American Institute of Physics. [DOI: 10.1063/1.2162184]

Under certain circumstances it is necessary to mix fluid in a Hele–Shaw cell, i.e., to mix viscous fluid between two closely spaced flat plates at a low Reynolds number (Re). An example of current interest is the improvement of microarray analysis for high-throughput screening of DNA.¹ One approach is to generate pressure-driven flow in the gap between the plates using sources and sinks produced by injecting and extracting fluid, respectively, through small holes in one of the plates. Time-periodic operation of sources and sinks has proven capable of mixing the fluid in a Hele–Shaw cell,^{1–4} and this fluid motion has been shown to have a significant effect on the speed and accuracy of microarray analysis.¹ The importance of microarray technology to genomics research⁵ makes it worthwhile to determine the parameters that optimize mixing in these pulsed source–sink systems.

The present work focuses on the specific source–sink configuration shown in Fig. 1, which has been applied to microarray analysis.¹ The aspect ratio of the domain is chosen so that it can be thought of as a standard microarray surface. Periodic fluid motion is generated by alternately pulsing the two source–sink pairs shown. During one “pulse,” flow is generated by simultaneous operation of one source and one sink with equal strength, i.e., by a source–sink pair. Total fluid volume is conserved by taking fluid extracted through a sink and reinjecting it through a source during the next pulse. For example, fluid extracted through the sink at $(z_-)_1$ is subsequently reinjected through the source at $(z_+)_2$. With the domain geometry and source–sink configuration fixed, the behavior of the system depends primarily on the *pulse volume*; that is, on how much fluid is injected (and extracted) through the active source (and sink) during each pulse.

This pulsed source–sink approach to mixing in a Hele–Shaw cell originated with the observation of chaotic advection in a two-dimensional (2D) potential flow with one source and one sink operated alternately in the unbounded plane.⁶ The use of a potential flow model is possible because the depth-averaged velocity in a Hele–Shaw flow can be rep-

resented by a velocity potential that is proportional to the local pressure.⁷ Chaotic advection, the phenomenon in which passive particles advected by a periodic velocity field exhibit chaotic trajectories, has proven to be a valuable tool for evaluating and predicting rapid mixing in a large number of laminar flows; for recent reviews see, e.g., Refs. 8 and 9. Thus, the appearance of chaotic advection in the model potential flow suggests that pulsed source–sink flow in a bounded Hele–Shaw cell will mix well, a connection that was first explored by Liepmann and coworkers.¹⁰

The utility of chaotic advection as a general guide in the development of a pulsed source–sink mixing device has been discussed previously.^{2,4} A detailed analysis of chaotic advection in such systems, however, has been presented only for the unbounded flow in Ref. 6. In this paper, we present such an analysis for the system shown in Fig. 1 and identify the

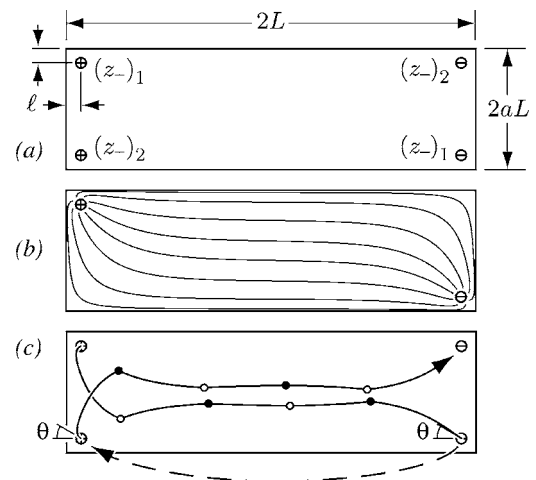


FIG. 1. (a) Domain geometry and source-sink locations, with $a=21/71$ and $\ell=5L/71$. The source locations are indicated by \oplus and labeled $(z_+)_i$ and the sink locations by \ominus and $(z_-)_i$. Source $(z_+)_1$ and sink $(z_-)_1$ are operated together as a pair, as are $(z_+)_2$ and $(z_-)_2$. In the model flow each source and sink is a *point* located at the center of its symbol. (b) Sample streamlines generated by steady operation of source-sink pair 1. (c) Trajectory of a particle leaving $(z_+)_1$ at $t=0$ for $\alpha=20\%$. Circles show the locations of the particle after each pulse. This particle is extracted through $(z_-)_1$ during the fifth pulse and reinjected through $(z_+)_2$ during the sixth pulse.

^{a)}Present address: Department of Mechanical Engineering, Purdue University, West Lafayette, IN 47907–2088.

values of pulse volume that generate optimal mixing protocol. This dynamical systems approach to mixing optimization has been used to examine several canonical mixing flows, including the partitioned pipe mixer,¹¹ the Kinex mixer,^{12,13} lid-driven cavity flow,¹⁴ and orthogonal shear flow on a torus.¹⁵ We employ a maximum entropy approach similar to that used in Ref. 15.

Different modeling techniques can be used to analyze transport in this pulsed source–sink system. Reference 4 suggests a three-dimensional (3D) finite-element model. We choose to proceed with a 2D potential flow model of the depth-averaged velocity. The motion generated by any source–sink pair is assumed to be steady, with the flow starting or stopping instantaneously when the source–sink pair is turned on or off, respectively. This model takes into account the viscous interaction of the fluid with the top and bottom plates but allows for fluid slip along the outer rectangular boundary. Despite the simplifications involved, we show that this model captures the mixing performance of this system reasonably well.

It is convenient to work in the complex plane, with the source and sink locations given by z_+ ($=x_+ + i y_+$) and z_- , respectively. The equations of motion can be determined by conformally mapping the upper half plane to the interior of a rectangle. The complex potential for flow driven by one source and one sink in the upper half plane is

$$F(z) = \phi + i\psi = \frac{q}{2\pi} [\log(z - z_+) + \log(z - z_+^*) - \log(z - z_-) - \log(z - z_-^*)], \quad (1)$$

where q is the strength of the source or sink and an asterisk denotes complex conjugation. The velocity potential is $\phi = \text{Re}(F)$, and $\psi = \text{Im}(F)$ is the streamfunction. The complex potential in a rectangular domain is then obtained by applying the Schwarz-Christoffel transformation¹⁶

$$w = f(z) = A \text{sn}^{-1}(z, k) + B, \quad (2a)$$

where $\text{sn}(z, k)$ is the Jacobian elliptic sine. The parameter k is determined from the aspect ratio of the domain, a , via

$$a = \frac{K(\sqrt{1-k^2})}{2K(k)}, \quad (2b)$$

where $K(k)$ is the complete elliptic integral of the first kind. If we choose the vertices of the rectangular domain to be located at $(\pm L, \pm aL)$, the parameters in (2a) are $A = L/K(k)$ and $B = -i aL$. The resulting complex potential for flow driven by one source and one sink in a rectangular domain is

$$F(z) = \frac{q}{2\pi} \{ \log[\sigma(z) - \sigma(z_+)] + \log[\sigma(z) - \sigma^*(z_+)] - \log[\sigma(z) - \sigma(z_-)] - \log[\sigma(z) - \sigma^*(z_-)] \}, \quad (3)$$

with $\sigma(x) = \text{sn}[(x/L + ia)K(k), k]$. Representative streamlines for this flow are shown in Fig. 1(b). Particle motion due to steady operation of a single source–sink pair is obtained by integrating numerically along a streamline. During the operation of several pulses a particle will follow a zigzag trajectory across the domain, as illustrated in Fig. 1(c).

During a single pulse, the active source–sink pair is operated steadily for time T , with the source (and sink) injecting (and extracting) fluid covering an area $A_p = qT$ in the rectangular domain, which has a total area A_c . The modeling results do not depend on the scale of the domain or the magnitude of the flow rate (as long as Re remains small), so we can work in terms of the dimensionless pulse area $\alpha = A_p/A_c$ and dimensionless time $\tau = qt/A_c$. With this scaling, the dimensionless pulse time, qT/A_c , is equal to α . Since the gap between plates in a Hele–Shaw cell is constant, α is also the fraction of the domain volume that is exchanged with each pulse; hence we will refer to α as the (dimensionless) pulse volume.

An important characteristic of this system is the method by which particles extracted through a sink are reinjected through a source. Experimental implementation can be accomplished with a “first in, last out” reinjection procedure (see, e.g., Ref. 3). In its simplest form, this procedure corresponds to collecting the extracted fluid in a tube, sliding the tube over to a source, and reinjecting the fluid into the domain. Neglecting any delay between extraction and reinjection, a particle that enters a sink during pulse n at time $(n-1)\alpha + \Delta$, with $0 < \Delta < \alpha$, will exit the appropriate source at time $(n+1)\alpha - \Delta$. The chaotic advection analysis also requires a one-to-one correspondence between a particle exiting the domain through a sink and a particle entering through a source. We assume that the “collection tube” is moved perfectly from sink to source, so that a particle enters the domain with the same angle θ at which it exited, as illustrated in Fig. 1(c). Other relationships are possible, of course, but we do not address any variations in this paper.

We are now ready to examine the influence of α on transport and mixing for piecewise constant operation of two source–sink pairs in a rectangular domain, with the flow governed at any given instant by (3) and with the above assumptions regarding reinjection. In the maximum entropy approach discussed in Ref. 15, consideration is restricted to those flows that exhibit mixing in the ergodic theory sense, which requires that (almost) every initial condition in the flow be subject to chaotic transport. The best mixing protocol is then determined for this set of flows by finding the one with maximum entropy. In this paper we expand the maximum entropy approach to include *decomposable* systems, such as our pulsed source–sink flow, that exhibit both regular and chaotic behavior. We can quantify disorder in these systems using the Kolmogorov (KS) entropy.¹⁷ In computing the KS entropy we need to consider Poincaré sections and Lyapunov exponents.

Poincaré sections are shown in Fig. 2 for several representative values of α . These plots are generated by recording the position of a passive particle in the domain after every period of operation, i.e., after every 2α . If pair 1 is operated first in the period, the solid circles in Fig. 1(c) contribute to the Poincaré section. For different values of α , the flow exhibits periodic points of various order, which is reflected in the *elliptic island* structure in the Poincaré sections. Particles with initial locations within these islands experience regular (nonchaotic) transport, while particles in the surrounding *chaotic sea* experience chaotic transport. We refer to the

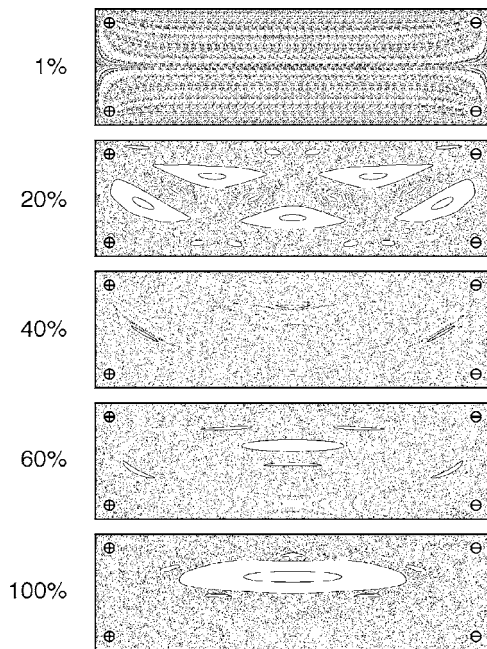


FIG. 2. Poincaré sections for the pulsed source-sink flow when pair 1 is operated first in the period. If pair 2 is instead operated first, or if particle positions are recorded on the half-period, the Poincaré sections are reflected about a horizontal axis. Panels are labeled according to the value of α . Initial particle locations vary between panels and are chosen to highlight island structure.

fraction of A_c that is covered by the chaotic sea as μ_s . All values of α investigated in the range $1\% \leq \alpha \leq 120\%$ generate chaotic transport over a large fraction of the domain, which is quantified in Fig. 3(a). Chaotic particle transport is accompanied by exponential stretching and folding of material lines in the flow, which rapidly increases the interface across which diffusion occurs and is generally expected to enhance mixing relative to regular advection. Thus, the greater the value of μ_s , the greater the potential for rapid mixing. Based strictly on this criterion, optimal mixing will be achieved in this system for $\alpha \approx 40\%$.

Some work on optimal mixing, such as that by Ling and co-workers,^{11,12} focuses exclusively on maximizing μ_s . The

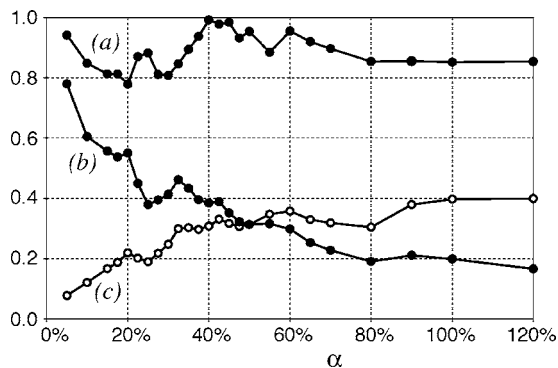


FIG. 3. (a) μ_s , the fraction of the domain area covered by the chaotic sea; (b) σ_τ , the maximum Lyapunov exponent for the flow; and (c) σ_n , the maximum Lyapunov exponent for the map. Each value was obtained by following multiple initial points in the chaotic sea for 2×10^5 or more periods.

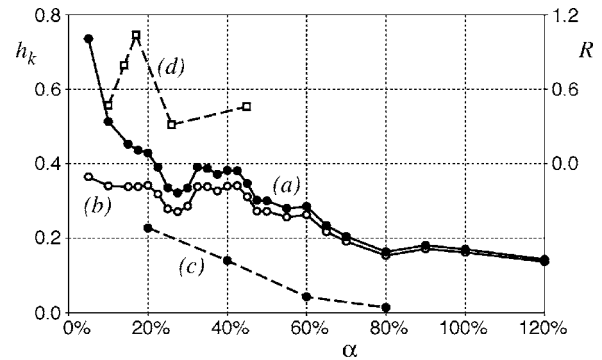


FIG. 4. KS entropy for (a) $\beta=0$ with fluid relocation, (b) $\beta=5\%$ with fluid relocation, and (c) $\beta=0$ without fluid relocation, where β is a dimensionless delay time between pulses. (d) The mixing rate, R , from the experiments in Ref. 3 with $\beta=0$.

presence of large elliptic islands will, of course, have a negative impact on global mixing; fluid in the chaotic sea may be mixed very rapidly, but fluid trapped in an elliptic island remains separate from the mixed fluid. However, nonideal behavior such as diffusion tends to quickly “smear out” small elliptic islands in most, if not all, practical implementations. Focusing exclusively on mixing protocols that maximize μ_s is too restrictive, or even incorrect, in some cases.

The primary limitation of a Poincaré section is that it gives no information quantifying how rapidly the fluid in the chaotic sea is stretched. The stretching rate of material lines is related to the maximum Lyapunov exponent for the flow, σ_τ , which quantifies the exponential rate of divergence in time of two neighboring points.¹⁷ Within an elliptic island a fluid element undergoes stretching that is, on average, only linear in time, and the Lyapunov exponents are zero. In the chaotic sea the Lyapunov exponents are nonzero, and on average the length l of a material line grows exponentially in time as $l \approx l_0 \exp(\sigma_\tau \tau)$, where l_0 is the initial (infinitesimal) length. Alternatively, the maximum Lyapunov exponent can be defined for the periodic map as $\sigma_n = 2\alpha \sigma_\tau$ in which case it quantifies the stretching rate per period of operation. The dependence of both σ_τ and σ_n on α for our system is shown in Figs. 3(b) and 3(c).

The general trend in this system is for the stretching rate per period, or σ_n , to increase with increasing α . However, larger pulse volumes require more time to complete, and as a result, the stretching rate in time, or σ_τ , generally decreases with increasing α . Since we wish to mix rapidly in time, we are interested primarily in σ_τ .

The information provided by the Poincaré sections and the Lyapunov exponents is combined in computing the KS entropy for the flow¹⁷

$$h_k = \mu_s \sigma_\tau. \quad (4)$$

Values of h_k for our pulsed source-sink flow are shown in Fig. 4(a). Optimal mixing in this system is expected for the value(s) of α that maximize h_k .

The trend in KS entropy suggests that small α optimizes mixing. However, closely examining the particle transport reveals that this is incorrect. In the limit as $\alpha \rightarrow 0$, particle motion approaches that due to the steady operation of two

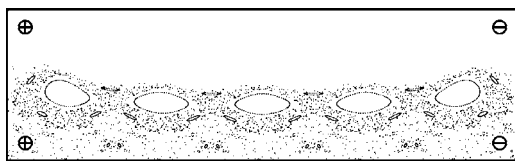


FIG. 5. Portion of the Poincaré section for $\alpha=10\%$ formed by following six particles in the bottom half of the domain for 750 periods.

sources and two sinks, which is fully regular. In the limiting case there is a streamline that divides the top and bottom halves of the domain. Pulsing the system removes this streamline, but for small α a barrier to transport remains in the time-averaged particle behavior. Fluid is stretched rapidly in each half of the domain but is not easily mixed between these two halves. This separation of the domain is quite apparent in the Poincaré section for $\alpha=1\%$ shown in Fig. 2. Even for $\alpha=10\%$, fluid is not mixed well between the top and bottom halves, as illustrated in Fig. 5. This segregation of the domain is not present for $\alpha \geq 15\%$. One approach to eliminating this segregation for small α is to switch the identification of $(z_-)_1$ and $(z_-)_2$, so that fluid extracted from the top half of the domain is reinjected into the bottom half, for example. This change is a straightforward modification of the current work and may be worth future consideration.

Maximum entropy leading to optimal mixing is thus obtained in this ideal pulsed source-sink system for $\alpha \approx 15\%$, with good mixing results expected for $15\% \leq \alpha \leq 20\%$ and $32.5\% \leq \alpha \leq 42.5\%$. Despite the simplifications employed in the model, these results are consistent with an experimental analysis,³ the results of which are summarized in Fig. 4(d). In these experiments, a small quantity of dye is introduced at $(z_+)_1$ and spread throughout the domain with a sequence of pulses. The *mixing rate*, R , characterizes the exponential decay rate in time of the coefficient of variation in intensity of the dye. In particular, the experiments show that, for the pulse volumes tested, optimal mixing is achieved when $\alpha \approx 17\%$, followed by $\alpha \approx 14\%$. Note that a mixing analysis based solely on μ_s incorrectly identifies $14\% \leq \alpha \leq 17\%$ as poor choices of pulse volume (see Fig. 3). The experiments also support our model prediction of poor mixing for $22.5\% < \alpha < 32.5\%$.

A practical implementation likely includes some delay between pulses to accommodate the logistics of the relocation procedure. If β is a nondimensional delay time, the total time for each pulse will be $\alpha + \beta$, giving $\sigma_\tau = \sigma_n / 2(\alpha + \beta)$. We expect β to be largely independent of the magnitude of α , and thus this delay will have the greatest effect on small α . Assuming $\beta=5\%$ gives the modified results for h_k shown in Fig. 4(b). As β increases, $32.5\% \leq \alpha \leq 42.5\%$ emerges as the parameter range for optimal mixing.

We find, then, that an analysis of particle transport and KS entropy in the model flow gives a prediction of mixing performance for the system in Fig. 1. Correspondence between this prediction and the experimental results in Ref. 3 allows one to use the results in Fig. 4 to identify, with reasonable confidence, an optimal mixing protocol for the prac-

tical system. This correspondence also supports the general use of a maximum entropy approach in determining optimal mixing protocols for decomposable systems that exhibit both chaotic and regular behavior.

We close with a comment on the importance of relocating the fluid prior to reinjection. In Fig. 4(c) we show the KS entropy for a few cases in which fluid extracted near a corner of the domain is reinjected through that same hole during a later pulse, as proposed in Ref. 4. The stretching per period in this system without relocation (not shown) is similar to that in ours, but each period of operation requires four pulses instead of two. Furthermore, for $\alpha \geq 60\%$ the domain is dominated by regular transport; for example, $\mu_s=13\%$ when $\alpha=80\%$. The net result is a substantial reduction in KS entropy, and we conclude that relocating the fluid prior to reinjection is crucial for optimizing mixing with two pulsed source-sink pairs in our rectangular domain.

The authors would like to thank E. Graybill for his assistance in generating data for Figs. 3 and 4, and I. Mezić for his helpful comments. This material is based upon work supported in part by the U. S. Army Research Laboratory and the U. S. Army Research Office under Contract No. W911NFO 410 349.

- ¹M. K. McQuain, K. Seale, J. Peek, T. Fisher, S. Levy, M. A. Stremler, and F. R. Haselton, "Chaotic mixer improves microarray hybridization," *Anal. Biochem.* **325**, 215 (2004).
- ²M. A. Stremler, F. R. Haselton, and H. Aref, "Designing for chaos: Applications of chaotic advection at the microscale," *Philos. Trans. R. Soc. London, Ser. A* **362**, 1019 (2004).
- ³B. A. Cola, D. K. Schaffer, T. S. Fisher, and M. A. Stremler, "A pulsed source-sink fluid mixing device," *J. Microelectromech. Syst.* **15**
- ⁴F. Raynal, F. Plaza, A. Beuf, P. Carrière, E. Souteyrand, J.-R. Martin, J.-P. Cloarec, and M. Cabrera, "Study of a chaotic mixing system for DNA chip hybridization chambers," *Phys. Fluids* **16**, L63 (2004).
- ⁵M. J. Heller, "DNA microarray technology: Devices, systems, and applications," *Annu. Rev. Biomed. Eng.* **4**, 129 (2002).
- ⁶S. W. Jones and H. Aref, "Chaotic advection in pulsed source-sink systems," *Phys. Fluids* **31**, 469 (1988).
- ⁷G. K. Batchelor, *An Introduction to Fluid Dynamics* (Cambridge University Press, Cambridge, 1967).
- ⁸H. Aref, "The development of chaotic advection," *Phys. Fluids* **14**, 1315 (1988).
- ⁹A theme issue on "Transport and mixing at the microscale," edited by J. M. Ottino and S. R. Wiggins, *Philos. Trans. R. Soc. London* **362**, 923–1129 (2004).
- ¹⁰J. Evans, D. Liepmann, and A. P. Pisano, "An Investigation of Micro Structures, Sensors, Actuators, Machines and Robots," in *Proceedings of the IEEE Tenth Annual International Workshop on Micro Electro Mechanical Systems*, 1997, p. 96.
- ¹¹F. H. Ling, "Chaotic mixing in a spatially periodic continuous mixer," *Phys. Fluids A* **5**, 2147 (1993).
- ¹²F. H. Ling and X. Zhang, "A numerical study on mixing in the Kenics static mixer," *Chem. Eng. Commun.* **136**, 119 (1995).
- ¹³E. S. Szalai and F. J. Muzzio, "Fundamental approach to the design and optimization of static mixers," *AIChE J.* **49**, 2687 (2003).
- ¹⁴M. Liu, F. J. Muzzio, and R. L. Peskin, "Quantification of mixing in aperiodic chaotic flows," *Chaos, Solitons Fractals* **4**, 869 (1994).
- ¹⁵D. D'Alessandro, M. Dahleh, and I. Mezić, "Control of mixing in fluid flow: a maximum entropy approach," *IEEE Trans. Autom. Control* **44**, 1852 (1999).
- ¹⁶T. A. Driscoll and L. N. Trefethen, *Schwarz-Christoffel Mapping* (Cambridge University Press, New York (2002).
- ¹⁷A. J. Lichtenberg and M. A. Leiberman, *Regular and Chaotic Dynamics*, 2nd ed. (Springer, New York, 1992).